

# First-Principles Study of Anharmonic Lattice Dynamics in Low Thermal Conductivity AgCrSe<sub>2</sub>: Evidence for a Large Resonant Four-Phonon Scattering

L. Xie,<sup>1</sup> J. H. Feng,<sup>1</sup> R. Li,<sup>2</sup> and J. Q. He<sup>1,\*</sup><sup>1</sup>Department of Physics, Southern University of Science and Technology, Shenzhen 518055, China<sup>2</sup>School of Environmental Science and Engineering, Southern University of Science and Technology, Shenzhen 518055, China

(Received 25 August 2020; accepted 13 November 2020; published 9 December 2020)

We report a study of the anharmonic lattice dynamics in low lattice thermal conductivity ( $\kappa_l$ ) material AgCrSe<sub>2</sub> by many-body perturbation theory. We demonstrate surprisingly giant four-phonon scattering exclusive for the heat-carrying transverse acoustic phonons due to large quartic anharmonicity and nondispersive phonon band structure, which lead to four-phonon Fermi resonance and breaks the classical  $\tau^{-1} \sim \omega^m T^n$  relation for phonon-phonon interactions. This strong resonant scattering extends over the Brillouin zone and substantially suppresses the thermal transport, even down to a low temperature of 100 K. The present results provide fundamental insights into the four-phonon resonant dynamics in the low- $\kappa_l$  system with flat phonon dispersions, i.e., cuprous halides and skutterudites.

DOI: 10.1103/PhysRevLett.125.245901

Phonon quasiparticles and their anharmonic interactions in solids have been a topic of intensive research, as they dominate fundamental thermodynamic properties, such as heat capacity and lattice thermal conductivity of a crystal. Materials with very high or very low thermal conductivities find important applications, such as thermal management of electronics, thermoelectricity [1], and thermal barrier coating. In low- $\kappa_l$  semiconductors or insulators, acoustic phonons are the main heat carriers and the most vital factor that limits  $\kappa_l$  [2]. This behavior can be understood from the high group velocity of acoustic phonons and the general  $\tau^{-1} \sim \omega^m T^n$  ( $\tau^{-1}$  is phonon scattering rate and  $m$  and  $n$  are integers determined by scattering mechanisms) for a phonon of frequency  $\omega$  at temperature  $T$  [1,3–7]. Given this general expression, the acoustic phonon scattering rate is usually lower than that of optical phonons, and the thermal transport is governed by acoustic phonons. To obtain lower  $\kappa_l$ , great efforts have been devoted to the modulation of acoustic phonons either by increasing the acoustic phonon scattering rate or by reducing the acoustic phonon group velocity. The former approach can be achieved via external routes of nanocrystallization [8,9] or hierarchical structuring [10,11]. Filling of rattling guest atoms can increase phonon scattering rate as well as reduce phonon group velocities simultaneously [12,13]. Meanwhile, internal degrees of freedom, such as rattling atoms [14,15], dynamic disorder [16,17], and static distortion [18], have also been revealed as possible means to suppress acoustic phonons transport. These findings inspire us to explore the intrinsic atomic dynamics and phonon interactions in low- $\kappa_l$  systems. In particular, in the crystals with weakly bonded, rattling constituents that exhibit flat and strongly anharmonic lattice potentials, quartic anharmonicity becomes nontrivial and new phenomenon or mechanism is expected [19].

Here, we demonstrate the emergence of giant transverse acoustic (TA) phonon resonant scattering in a low- $\kappa_l$  model system AgCrSe<sub>2</sub> by anharmonic lattice dynamics calculations. We find that, even down to a low temperature of 100 K, the TA phonons in AgCrSe<sub>2</sub> are overwhelmed exclusively by resonating four-phonon scattering over three-phonon scattering with an exceptionally large scattering rate ratio  $\tau_{4\text{ph}}^{-1}/\tau_{3\text{ph}}^{-1} \sim 14$ , and the  $\tau^{-1} \sim \omega^m T^n$  rule breaks down. Our results not only highlight the importance of quartic anharmonicity, but also emphasize the critical role of flat TA phonon dispersions that lead to Fermi resonance. With this four-phonon resonant scattering, the low- $\kappa_l$  behavior of AgCrSe<sub>2</sub> well below room temperature (RT) is also explained.

AgCrSe<sub>2</sub> is a superionic conductor [20] and it undergoes an order-to-disorder phase transition at  $T_c \sim 475$  K [21]. Figure 1(a) displays the order phase structure of AgCrSe<sub>2</sub> (space group  $R3m$ ), in which Ag<sup>+</sup> ions prefer one of the equivalent lattice sites in between the rigid CrSe<sub>2</sub> octahedra. While the ultralow  $\kappa_l$  ( $\sim 0.4$ – $0.5$  W m<sup>-1</sup>K<sup>-1</sup>) and

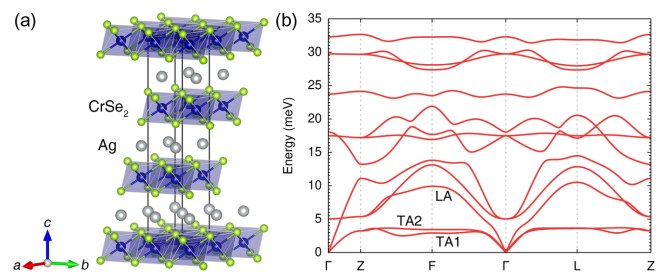


FIG. 1. (a) Atomic structure of low-temperature ordered phase AgCrSe<sub>2</sub> (space group  $R3m$ ). (b) Calculated phonon dispersion of AgCrSe<sub>2</sub> at 100 K.

phonon-liquid behavior of AgCrSe<sub>2</sub> above  $T_c$  have attracted increasing interest [17,22–25], its unusual thermal transport property well below  $T_c$  is intriguing as well as its  $\kappa_l$  is already very low at 100–300 K, about  $\sim 0.4\text{--}1.0 \text{ W m}^{-1} \text{ K}^{-1}$  and no longer follows the general  $\kappa_l \sim T^{-1}$  rule [22]. These abnormal behaviors imply a critical role of higher-order anharmonicity at low temperature, but are still not well studied yet.

Figure 1(b) displays the phonon dispersion of AgCrSe<sub>2</sub> (R3m) at 100 K, calculated by the software TDEP [26,27]. The most important feature of Fig. 1(b) is that the TA branches ( $\sim 3 \text{ meV}$  for TA1 and  $\sim 3.5 \text{ meV}$  for TA2) are almost flat throughout the Brillouin zone. This non-dispersive feature is consistent with previous findings [22] and implies that a large fraction of TA phonons is localized with low group velocities. As shown in Fig. S1 of the Supplemental Material [28], the phonon dispersions at 200 and 300 K exhibit similar nondispersive feature as well.

Next, we show that these localized modes are dominated by four-phonon interactions by anharmonic lattice dynamics calculations. The calculations were performed by Vienna *ab initio* software package (VASP) [29,30] and our modified TDEP code [26,27] (see Supplemental Material [28] for more technical details). The phonon dynamics are investigated by the phonon spectral function  $S_{\vec{k},s}(\omega)$  [4,6,32]

$$S_{\vec{k},s}(\omega) = \frac{2\omega_{\vec{k},s} \Gamma_{\vec{k},s}(\omega)}{[\omega^2 - \omega_{\vec{k},s}^2 - 2\omega_{\vec{k},s} \Delta_{\vec{k},s}(\omega)]^2 + 4\omega_{\vec{k},s}^2 \Gamma_{\vec{k},s}^2(\omega)}, \quad (1)$$

where  $\omega_{\vec{k},s}$  is the eigenfrequency of phonon mode  $(\vec{k}, s)$ , and  $\Delta_{\vec{k},s}(\omega)$  and  $\Gamma_{\vec{k},s}(\omega)$  are the real and imaginary part of phonon self-energy  $\Sigma_{\vec{k},s}(\omega) = \Delta_{\vec{k},s}(\omega) + i\Gamma_{\vec{k},s}(\omega)$ , respectively.  $\Sigma_{\vec{k},s}(\omega)$  describes the renormalization of a bare phonon by frequency shift  $\Delta$  and linewidth broadening  $\Gamma$ . For simplicity, we approximate  $\Sigma_{\vec{k},s}(\omega)$  by its low-order perturbations

$$\begin{aligned} \Sigma_{\vec{k},s}(\omega) &\approx \Sigma_{\vec{k},s}^{(1)}(\omega) + \Sigma_{\vec{k},s}^{(2)}(\omega) \\ &= [\Delta_{\vec{k},s}^{(1)}(\omega) + i\Gamma_{\vec{k},s}^{(1)}(\omega)] + [\Delta_{\vec{k},s}^{(2)}(\omega) + i\Gamma_{\vec{k},s}^{(2)}(\omega)]. \end{aligned} \quad (2)$$

The first bracket set in Eq. (2) is the first- and second-order perturbations as calculated from the loop and bubble diagrams [4]. Its imaginary part  $\Gamma_{\vec{k},s}^{(1)}(\omega)$  is essentially determined by three-phonon and isotopic scattering [4,32]. The second bracket set in Eq. (2) is associated with four-phonon interactions [35,36]. The expressions for these self-energy terms can be found in the Supplemental Material, Sec. 2 [28]. Figure 2 displays the calculated total spectral function  $S_{\vec{k}}(\omega) = \sum_s S_{\vec{k},s}(\omega)$  (at 100 K) along the high-symmetry directions in the Brillouin zone. The  $S_{\vec{k}}(\omega)$  without four-phonon interactions are also given by letting

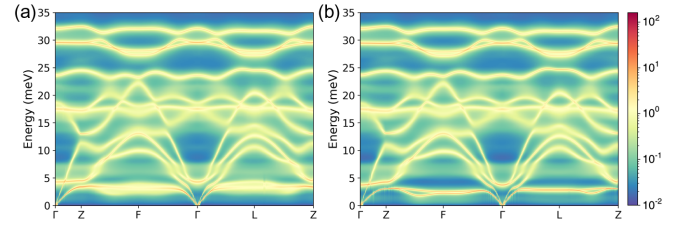


FIG. 2. Theoretical spectral function  $S_{\vec{k}}(\omega)$  (in logarithm scale) of AgCrSe<sub>2</sub>, as calculated at 100 K (a) with and (b) without second-order quartic anharmonic perturbations  $\Sigma^{(2)}$ . Note the dramatic change of the low-lying transverse acoustic phonons.

$\Sigma_{\vec{k},s}(\omega) = \Sigma_{\vec{k},s}^{(1)}(\omega)$ . Obviously, the low-lying TA phonons are modulated substantially by four-phonon interactions. With  $\Sigma_{\vec{k},s}^{(2)}(\omega)$ , the  $S_{\vec{k}}(\omega)$  of TA phonons become much broadened and diffuse, indicating dominating four-phonon scattering over three-phonon scattering at 100 K. In addition, the frequency shift to lower energy by  $\Delta_{\vec{k},s}^{(1)}(\omega)$  [Fig. 2(b)] is effectively compensated by  $\Delta_{\vec{k},s}^{(2)}(\omega)$ . For the remaining part of  $S_{\vec{k}}(\omega)$  that corresponds to longitudinal acoustic (LA) and optical modes, there are no marked differences between the  $S_{\vec{k}}(\omega)$  with or without four-phonon interactions  $\Sigma_{\vec{k},s}^{(2)}(\omega)$  except for a slight broadening. The same phonon line shape feature is also observed at an increasing temperature of 200 and 300 K (Fig. S3 [28]), highlighting the persistent strong four-phonon interactions up to RT.

The significant renormalization of TA phonons can be seen more clearly in Fig. 3, in which the temperature-dependent  $S_{\vec{k},s}(\omega)$  of TA phonons, along with the LA phonon as a reference, at representative reciprocal point ( $F$  point) with and without  $\Sigma_{\vec{k},s}^{(2)}(\omega)$  are plotted. The vertical bars in Fig. 3 indicate the eigenfrequencies  $\omega_{\vec{k},s}$  of “bare” phonons and clear phonon spectral function shifts away from  $\omega_{\vec{k},s}$  could be observed. We have also plotted the  $\Sigma_{\vec{k},s}(\omega)$  of acoustic phonons as a function of temperatures in detail in Fig. S6 [28]. A further discussion of these  $\Sigma_{\vec{k},s}(\omega)$  and their contributions to  $S_{\vec{k},s}(\omega)$  is given in the Supplemental Material, Sec. 2 [28].

As the phonon scattering rate  $\tau^{-1}$ , or the inverse of phonon life time  $\tau$ , is related to phonon self-energy  $\Gamma$  as  $\tau^{-1} = 2\Gamma$  [4], the TA phonon scattering rates for the four- and three-phonon process at  $F$  point can be evaluated directly from their phonon self-energy  $\Gamma_{\vec{k},s}(\omega)$  (see Fig. S6 [28]). It is found that  $\tau_{4\text{ph}}^{-1}$  of TA1 (TA2) mode increases from  $\sim 1.82$  (0.68)  $\text{ps}^{-1}$  at 100 K to  $\sim 4.25$  (1.90)  $\text{ps}^{-1}$  at 300 K, while  $\tau_{3\text{ph}}^{-1}$  of TA1 (TA2) mode is only  $\sim 0.15$  (0.21)  $\text{ps}^{-1}$  at 100 K and  $\sim 0.36$  (0.38)  $\text{ps}^{-1}$  at 300 K. As a result, the ratio between these two scattering rates  $\tau_{4\text{ph}}^{-1}/\tau_{3\text{ph}}^{-1}$  at 100–300 K are tremendous,  $\sim 12\text{--}14$  for TA1 mode and  $\sim 3\text{--}6$  for TA2 mode, respectively. These

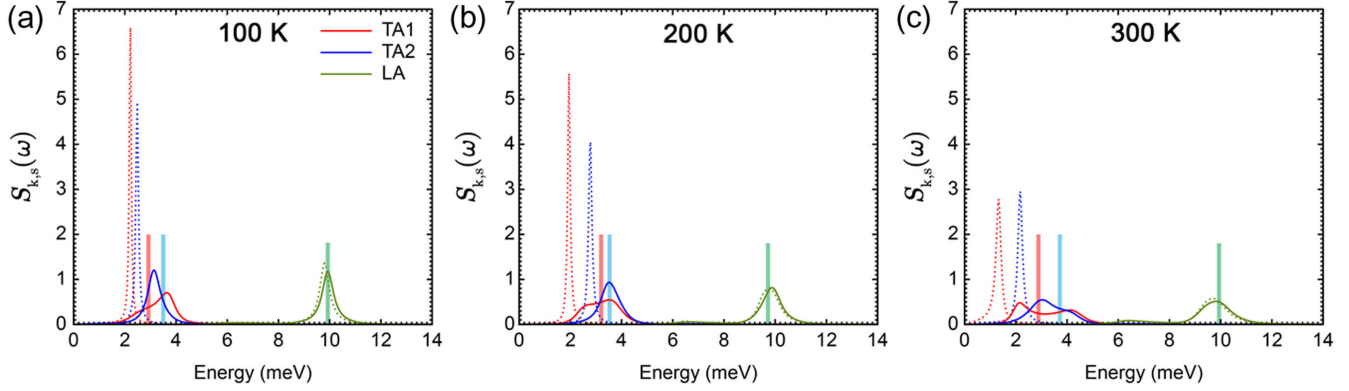


FIG. 3. Temperature dependent spectral function  $S_{\vec{k},s}^{-1}(\omega)$  (solid line calculated with  $\Sigma_{\vec{k},s}^{-1} = \Sigma_{\vec{k},s}^{(1)} + \Sigma_{\vec{k},s}^{(2)}$ ; dashed line calculated with  $\Sigma_{\vec{k},s}^{-1} = \Sigma_{\vec{k},s}^{(1)}$ ) of the acoustic phonons at  $F$  point, as calculated at (a) 100, (b) 200, and (c) 300 K, respectively. The colored vertical bars indicate the phonon eigenfrequency  $\omega_{\vec{k},s}^{-}$  of each phonon mode (red, TA1; blue, TA2; green, LA). The phonon linewidth broadening and frequency shift due to the four-phonon interactions  $\Sigma_{\vec{k},s}^{(2)}$  can be clearly observed.

results are in agreement with inelastic neutron scattering, by which  $2\Gamma$  was determined as 1.2–2.0 meV [17]. Here, it must be noted that the  $\tau_{4\text{ph}}^{-1}$  of TA phonons is so large that they are comparable to those of optical phonons. More surprisingly,  $\tau_{4\text{ph}}^{-1}$  is even comparable to  $\omega_{\vec{k},s}^{-}$  at 300 K as  $\omega_{\vec{k},s}^{-}\tau_{4\text{ph}} = 1.07 \approx 1$ . In this case, the phonon quasiparticle picture is no longer valid [45,46]. In fact, as shown in Fig. 3, the  $S_{\vec{k},s}^{-1}(\omega)$  of TA phonons are renormalized considerably. For TA1 mode, a clear shoulder structure appears at 100–200 K and its shape is not as well defined as that of phonon quasiparticles, e.g., LA phonon. At 300 K,  $S_{\vec{k},s}^{-1}(\omega)$  even splits into two diffuse peaks and the quasiparticle picture breaks down completely. To our best knowledge, such an anomalous two-mode behavior is rare. One example is CuCl, in which a double-peak structure forms as a result of Fermi resonance [47]. In our previous work, it was also demonstrated that a two-mode feature appears in BaTiO<sub>3</sub> due to the coupling between phonons and pseudospins [48]. Recently, a similar two-mode behavior and breakdown of the quasiparticle picture have been discovered in SnSe [49] and SnS [50] as well. These unusual behaviors were ascribed to the contributions from phonon self-energy beyond the third order, as in our case. For TA2 phonon, its  $S_{\vec{k},s}^{-1}(\omega)$  at 100–200 K is of the conventional shape of a Lorentzian function owing to the weaker four-phonon interactions. A small shoulder starts to emerge at 300 K with increasing  $\Sigma_{\vec{k},s}^{-1}(\omega)$ . Overall, the strong four-phonon interactions of the TA phonons are general throughout the Brillouin zone and the results at other reciprocal points are given in the Supplemental Material, Sec. 2 [28].

The strikingly enormous four-phonon scattering rates exclusive for the TA phonons at low temperatures cannot be explained by the classical  $\tau^{-1} \sim \omega^m T^n$  relation [40]. For example, Ecsedy and Klemens had calculated the  $\tau_{4\text{ph}}^{-1}/\tau_{3\text{ph}}^{-1}$

ratio with  $\tau_{4\text{ph}}^{-1} \sim \omega^2 T^2$  [40]. They found that  $\tau_{4\text{ph}}^{-1}/\tau_{3\text{ph}}^{-1}$  is typically very small, only  $3 \times 10^{-2}$  at 1000 K. According to Feng *et al.* [7], four-phonon scattering is expected to be more pronounced for optical phonons as  $\tau_{4\text{ph}}^{-1} \sim \omega^4 T^2$ . The gigantic four-phonon scattering of the TA phonons in AgCrSe<sub>2</sub> can be ascribed to (1) strong quartic anharmonicity and (2) the unique flat TA phonon dispersions that lead to Fermi resonance. Following the approach of Feng *et al.* [7], we can estimate the relative strength of the quartic anharmonicity  $|\Phi_4/\Phi_3|^2/|\Phi_2|$  from the  $n$ th-order force constant  $\Phi_n$ . Using the interatomic force constants derived at 100 K, we found that  $|\Phi_4/\Phi_3|^2/|\Phi_2|$  of the Ag atom is  $\sim 4.27$ . As a benchmark, the  $|\Phi_4/\Phi_3|^2/|\Phi_2|$  of the B atom in the well-known BAs crystal with significant four-phonon scattering is only 0.122 [7]. In addition to the strong quartic anharmonicity, the flat TA phonon branches are of great importance as well. As pictorially drawn in Fig. 4,

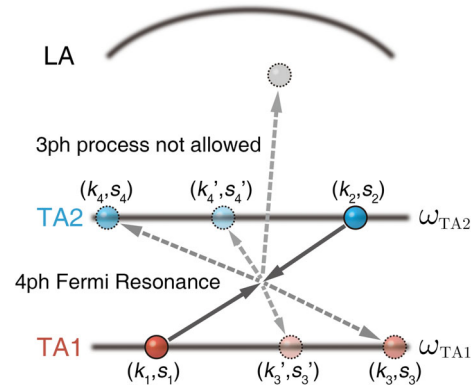


FIG. 4. Schematic diagram showing the four-phonon recombination process or four-phonon Fermi resonance facilitated by flat transverse acoustic phonon dispersions. In comparison, the three-phonon scattering process is restricted by conservation of momentum and energy.

any TA phonon ( $\vec{k}_1, s_1$ ) can readily combine with another TA phonon ( $\vec{k}_2, s_2$ ) and create two new TA phonons ( $\vec{k}_3, s_3$ ) and ( $\vec{k}_4, s_4$ ) by the four-phonon recombination process [7,51] because the energy conservation ( $\omega_{\vec{k}_1, s_1} + \omega_{\vec{k}_2, s_2} = \omega_{\vec{k}_3, s_3} + \omega_{\vec{k}_4, s_4}$ ) is satisfied automatically. Meanwhile, the conservation of momentum requires

$$\vec{k}_1 + \vec{k}_2 = \vec{k}_3 + \vec{k}_4 + \vec{G}, \quad (3)$$

where  $\vec{G}$  is a reciprocal lattice vector. Provided that the two TA phonon branches are parallel, Eq. (3) is very easy to fulfill since we can always find a  $\vec{k}_4$  for any given  $\vec{k}_3$ . In the simplest 1D case,  $\vec{k}_1 - \vec{k}_4$  form a parallelogram. As a result, the cumulative four-phonon scattering phase space by summing all the  $\vec{k}_2, \vec{k}_3$ , and  $\vec{G}$  is enormous. In comparison, the three-phonon scattering is limited because only specific reciprocal points can satisfy both momentum conservation  $\vec{k}_1 + \vec{k}_2 = \vec{k}_3 + \vec{G}$  and energy conservation simultaneously. It should be remarked that, besides the recombination process as described by Eq. (3), four-phonon absorption and emission processes contribute to phonon scattering as well. However, similar to three-phonon scattering, these processes are restricted by momentum and energy conservation and thus are less significant. The above result is exactly Fermi resonance. The basic idea is that the frequency of three-phonon density of states (DOS) at high density coincides with the phonon eigenfrequency and the three-phonon DOS are coupled to the one-phonon DOS by quartic anharmonicity [47]. Neglecting the four-phonon accumulation and emission processes, the three-phonon DOS for the dispersion shown in Fig. 4 can be written as

$$\begin{aligned} 3\text{phDOS}(\omega) = & \frac{1}{N_k} \sum_{\vec{k}_2, \vec{k}_3, \vec{k}_4, \vec{G}} \sum_{s_2, s_3, s_4} \delta(\omega + \omega_{\vec{k}_2, s_2} - \omega_{\vec{k}_3, s_3} - \omega_{\vec{k}_4, s_4}) \\ & \times \delta_{\vec{k}_1, \vec{k}_2, \vec{k}_3 + \vec{k}_4 + \vec{G}}, \end{aligned} \quad (4)$$

where  $\delta$  is the Dirac  $\delta$  function and  $N_k$  is the total number of  $k$  points. Equation (4) spikes exactly at  $\omega_{\text{TA1}}$  and  $\omega_{\text{TA2}}$ . Thus, four-phonon Fermi resonance occurs.

The significantly increased TA phonon scattering together with its low velocity explain the unusual  $\kappa_l$  of AgCrSe<sub>2</sub> below RT qualitatively. A quantitative comparison between theories and experiments is also of interest. However, we are aware that such an attempt is beyond current kinetic theories because either the relaxation time approximation [52] or the phonon Boltzmann equation [53,54] are only valid in the limit of weak anharmonicity, i.e.,  $\omega\tau \gg 1$  [45,46,55,56]. In the case of strong anharmonicity, whether the scattering rates (or the lifetime) of a phonon can still be determined by  $\tau^{-1} = 2\Gamma(\omega_{\vec{k}, s})$  is a question. For example, as we have already observed in the  $S_{\vec{k}, s}(\omega)$  of TA phonons, there is no unambiguous way to define the linewidths of these phonons because of strong phonon renormalization. To resolve this issue, a formalism

of the phonon spectral distribution beyond the quasiparticle picture is necessary. Anyhow, it is still of great interest to compare experiments with theories semiquantitatively. We have provided the calculation results based on the Boltzmann transport equation and it does confirm that  $\kappa_l$  is substantially reduced by four-phonon scattering (see Supplemental Material, Sec. 3 [28] for details).

In addition to a reduced  $\kappa_l$ , the four-phonon Fermi resonance has further implications. First of all, it provides a natural and self-consistent explanation of the phenomenological ‘‘resonant’’ scattering proposed in filled skutterudites [13,44], Cu<sub>3</sub>SbSe<sub>3</sub> [57], and  $\alpha$ -MgAgSb [58]. The rattling dynamics of loosely bounded atoms, whether they are hosts or guests, can be fully incorporated into anharmonic lattice dynamics when a four-phonon process is considered. Indeed, our calculations confirm that the resonant scattering in Yb-filled FeSb<sub>3</sub> does come from four-phonon Fermi resonance (see Supplemental Material, Sec. 4 [28]). More importantly, the four-phonon Fermi resonance provides a universal picture of how localized Einstein-like oscillators are coupled to each other resonantly in crystals via quartic anharmonicity. These couplings should not only be restricted to acoustic-acoustic phonon interactions, but are also valid for acoustic-optical and optical-optical phonon interactions [59,60]. The prototypical crystals with characteristic nondispersive phonon band structures are all possible candidates to search for such interactions and low- $\kappa_l$  property. Actually, we have found that AgCrS<sub>2</sub>, cuprous halides (CuCl, CuBr, CuI), Cu<sub>2</sub>O, SnSe, and PbTiO<sub>3</sub> are such systems with sizable four-phonon scattering. The phonon dispersions of these materials are given in the Supplemental Material, Sec. 4 [28] and detailed calculations of their four-phonon interactions will be reported elsewhere. Cu<sub>2</sub>Se is another potential system as well. Neutron scattering experiments of Cu<sub>1.8</sub>Se showed that its TA phonons do have dispersionless characteristics and extremely broadened phonon linewidths [61,62].

In conclusion, we have demonstrated the emergence of giant acoustic phonon resonant scattering in the model system AgCrSe<sub>2</sub> by anharmonic lattice dynamics calculations. Our results highlight the importance of strong quartic anharmonicity and the crucial role of characteristic flat phonon dispersion, which results in four-phonon Fermi resonance and the breakdown of the general  $\tau^{-1} \sim \omega^m T^n$  rule well below RT. We believe our findings are universal and applicable to a number of low- $\kappa_l$  materials, especially those with characteristic nondispersive phonon band structure and rattling dynamics. These results provide new insights into crystalline materials with anomalous  $\kappa_l$  and lead to a rational strategy to develop new low- $\kappa_l$  materials.

This work is supported by the National Natural Science Foundation of China (Grants No. 11934007, 11874194 and No. 51632005), the Natural Science Foundation of Guangdong Province (Grant No. 2015A030308001), the

Leading Talents of Guangdong Province Program (Grant No. 00201517), the Science and Technology Innovation Committee Foundation of Shenzhen (Grants No. JCYJ20190809145205497 and No. KQTD20160222619565991) and Center for Computational Science and Engineering of Southern University of Science and Technology.

\*Corresponding author.  
he.jq@sustech.edu.cn

- [1] H. J. Goldsmid, in *Introduction to Thermoelectricity* (Springer, Berlin, Heidelberg, 2010), p. 1.
- [2] D. G. Cahill and R. O. Pohl, *Annu. Rev. Phys. Chem.* **39**, 93 (1988).
- [3] J. Callaway, *Phys. Rev.* **113**, 1046 (1959).
- [4] A. A. Maradudin and A. E. Fein, *Phys. Rev.* **128**, 2589 (1962).
- [5] M. G. Holland, *Phys. Rev.* **132**, 2461 (1963).
- [6] R. A. Cowley, *Rep. Prog. Phys.* **31**, 123 (1968).
- [7] T. Feng, L. Lindsay, and X. Ruan, *Phys. Rev. B* **96**, 161201 (R) (2017).
- [8] B. Poudel *et al.*, *Science* **320**, 634 (2008).
- [9] C. J. Vineis, A. Shakouri, A. Majumdar, and M. G. Kanatzidis, *Adv. Mater.* **22**, 3970 (2010).
- [10] K. Biswas, J. He, I. D. Blum, C.-I. Wu, T. P. Hogan, D. N. Seidman, V. P. Dravid, and M. G. Kanatzidis, *Nature (London)* **489**, 414 (2012).
- [11] H. J. Wu, L. D. Zhao, F. S. Zheng, D. Wu, Y. L. Pei, X. Tong, M. G. Kanatzidis, and J. Q. He, *Nat. Commun.* **5**, 4515 (2014).
- [12] B. C. Sales, D. Mandrus, and R. K. Williams, *Science* **272**, 1325 (1996).
- [13] T. Takabatake, K. Suekuni, T. Nakayama, and E. Kaneshita, *Rev. Mod. Phys.* **86**, 669 (2014).
- [14] M. K. Jana, K. Pal, A. Warankar, P. Mandal, U. V. Waghmare, and K. Biswas, *J. Am. Chem. Soc.* **139**, 4350 (2017).
- [15] M. Dutta, S. Matteppanavar, M. V. D. Prasad, J. Pandey, A. Warankar, P. Mandal, A. Soni, U. V. Waghmare, and K. Biswas, *J. Am. Chem. Soc.* **141**, 20293 (2019).
- [16] H. Liu, X. Shi, F. Xu, L. Zhang, W. Zhang, L. Chen, Q. Li, C. Uher, T. Day, and G. J. Snyder, *Nat. Mater.* **11**, 422 (2012).
- [17] B. Li *et al.*, *Nat. Mater.* **17**, 226 (2018).
- [18] X. Li *et al.*, *Nat. Commun.* **11**, 942 (2020).
- [19] Y. Xia, K. Pal, J. He, V. Ozoliņš, and C. Wolverton, *Phys. Rev. Lett.* **124**, 065901 (2020).
- [20] D. W. Murphy, *J. Electrochem. Soc.* **124**, 1268 (1977).
- [21] A. Van Der Lee and G. A. Wiegers, *J. Solid State Chem.* **82**, 216 (1989).
- [22] F. Damay, S. Petit, S. Rols, M. Braendlein, R. Daou, E. Elkaim, F. Fauth, F. Gascoin, C. Martin, and A. Maignan, *Sci. Rep.* **6**, 23415 (2016).
- [23] L. Xie, D. Wu, H. Yang, Y. Yu, Y. Wang, and J. He, *J. Mater. Chem. C* **7**, 9263 (2019).
- [24] J. Ding *et al.*, *Proc. Natl. Acad. Sci. U.S.A.* **117**, 3930 (2020).
- [25] C. Wang and Y. Chen, *npj Comput. Mater.* **6**, 26 (2020).
- [26] O. Hellman, I. A. Abrikosov, and S. I. Simak, *Phys. Rev. B* **84**, 180301(R) (2011).
- [27] O. Hellman, P. Steneteg, I. A. Abrikosov, and S. I. Simak, *Phys. Rev. B* **87**, 104111 (2013).
- [28] See Supplemental Material at <http://link.aps.org/supplemental/10.1103/PhysRevLett.125.245901> for details on the perturbation theory for anharmonic lattice dynamics, calculation methods, and further discussions, which includes Refs. [29–44].
- [29] G. Kresse and J. Furthmüller, *Phys. Rev. B* **54**, 11169 (1996).
- [30] G. Kresse and J. Furthmüller, *Comput. Mater. Sci.* **6**, 15 (1996).
- [31] P. E. Blöchl, *Phys. Rev. B* **50**, 17953 (1994).
- [32] N. Shulumba, O. Hellman, and A. J. Minnich, *Phys. Rev. B* **95**, 014302 (2017).
- [33] A. Togo and I. Tanaka, *Scr. Mater.* **108**, 1 (2015).
- [34] F. Eriksson, E. Fransson, and P. Erhart, *Adv. Theory Simul.* **2**, 1800184 (2019).
- [35] R. S. Tripathi and K. N. Pathak, *Il Nuovo Cimento B* (1971–1996) **21**, 289 (1974).
- [36] P. Procacci, G. Cardini, R. Righini, and S. Califano, *Phys. Rev. B* **45**, 2113 (1992).
- [37] M. Balkanski, R. F. Wallis, and E. Haro, *Phys. Rev. B* **28**, 1928 (1983).
- [38] S.-i. Tamura, *Phys. Rev. B* **27**, 858 (1983).
- [39] I. Pomeranchuk, *Phys. Rev.* **60**, 820 (1941).
- [40] D. J. Ecsedy and P. G. Klemens, *Phys. Rev. B* **15**, 5957 (1977).
- [41] O. Hellman and D. A. Broido, *Phys. Rev. B* **90**, 134309 (2014).
- [42] F. Gascoin and A. Maignan, *Chem. Mater.* **23**, 2510 (2011).
- [43] D. Wu, S. Huang, D. Feng, B. Li, Y. Chen, J. Zhang, and J. He, *Phys. Chem. Chem. Phys.* **18**, 23872 (2016).
- [44] Y. Wang, H. Yang, W. Qiu, J. Yang, J. Yang, and W. Zhang, *Phys. Rev. B* **98**, 054304 (2018).
- [45] D. G. Cahill, S. K. Watson, and R. O. Pohl, *Phys. Rev. B* **46**, 6131 (1992).
- [46] P. B. Allen, *Phys. Rev. B* **92**, 064106 (2015).
- [47] G. Kanellis, W. Kress, and H. Bilz, *Phys. Rev. Lett.* **56**, 938 (1986).
- [48] L. Xie, Y. L. Li, R. Yu, and J. Zhu, *J. Appl. Phys.* **109**, 054101 (2011).
- [49] U. Aseginolaza, R. Bianco, L. Monacelli, L. Paulatto, M. Calandra, F. Mauri, A. Bergara, and I. Errea, *Phys. Rev. Lett.* **122**, 075901 (2019).
- [50] U. Aseginolaza, R. Bianco, L. Monacelli, L. Paulatto, M. Calandra, F. Mauri, A. Bergara, and I. Errea, *Phys. Rev. B* **100**, 214307 (2019).
- [51] T. Feng and X. Ruan, *Phys. Rev. B* **93**, 045202 (2016).
- [52] P. Carruthers, *Rev. Mod. Phys.* **33**, 92 (1961).
- [53] R. Peierls, R. E. Peierls, R. E. Peierls, and O. U. Press, *Quantum Theory of Solids* (Clarendon Press, Oxford, 1955).
- [54] M. Omini and A. Sparavigna, *Phys. Rev. B* **53**, 9064 (1996).
- [55] G. Kirczenow, *Ann. Phys. (N.Y.)* **125**, 1 (1980).
- [56] R. J. Hardy, *J. Math. Phys.* **7**, 1435 (1966).
- [57] W. Qiu, L. Xi, P. Wei, X. Ke, J. Yang, and W. Zhang, *Proc. Natl. Acad. Sci. U.S.A.* **111**, 15031 (2014).
- [58] P. Ying, X. Li, Y. Wang, J. Yang, C. Fu, W. Zhang, X. Zhao, and T. Zhu, *Adv. Funct. Mater.* **27**, 1604145 (2017).
- [59] X. Yang, T. Feng, J. S. Kang, Y. Hu, J. Li, and X. Ruan, *Phys. Rev. B* **101**, 161202(R) (2020).
- [60] X. Yang, T. Feng, J. Li, and X. Ruan, *Phys. Rev. B* **100**, 245203 (2019).
- [61] S. A. Danilkin, M. Yethiraj, and G. J. Kearley, *J. Phys. Soc. Jpn.* **79**, 25 (2010).
- [62] S. A. Danilkin, A. N. Skomorokhov, A. Hoser, H. Fuess, V. Rajevac, and N. N. Bickulova, *J. Alloys Compd.* **361**, 57 (2003).